24th COBEM - 2017

24th ABCM International Congress of Mechanical Engineering
December 3-8, 2017, Curitiba, PR, Brazil

COBEM-2017-2655
DYNAMICS OF A SELF-FOLDING CYLINDRICAL SYSTEM ACTUATED BY SMA

Guilherme Vieira Rodrigues
Larissa Maciel da Fonseca
Marcelo Amorim Savi
Universidade Federal do Rio de Janeiro, COPPE - Department of Mechanical Engineering, MECANON - Center for Nonlinear Mechanics, Rio de Janeiro, RJ – Brazil
guilherme_@live.co.uk; larissamaciel.lah@gmail.com; savi@mecanica.ufrj.br

Alberto Paiva
Universidade Federal Fluminense, Department of Mechanical Engineering, Volta Redonda, RJ - Brazil
paiva.ufrj@gmail.com

Abstract. *Self-folding structures based on origami art have inspired many design projects in engineering field. Such structures are able to change their shape and size expressively. Smart materials are widely employed as actuators. Shape Memory Alloys (SMA) belong to this class of materials and provide a wide field of displacement or force actuation by varying their temperature. Dynamics of a cylindrical shaped origami structure with the ability of changing its radius is investigated in this work. Actuation is provided by torsional SMA wires placed on origami creases. A polynomial constitutive model is considered to describe the thermomechanical behavior of the actuators. A 1-DOF model is established based on geometric assumptions. The system behavior is investigated under thermomechanical loadings. Constitutive and geometric nonlinearities enriches the dynamic responses of the system.*

Keywords: *self-folding structures, origami-inspired devices, shape memory alloys, nonlinear dynamics, chaos.*

1. INTRODUCTION

The ancient art of origami, or paper folding, has inspired several innovative design projects of engineering systems. This technique enables one to create a three-dimensional geometry by following a sequence of folds in a sheet of paper. Some of these geometries are able to change its shape and size expressively, being so employed in self-folding systems.

The contracting-expanding ability of origami-inspired structures motivates their use in aerospace applications. Miura (1994) is one of the first researchers to present a practical use of an origami technique in engineering, applying it to a foldable solar panel. It assists the solution of the problem of space restrictions during transportation processes because the folded configuration is very compacted and its foldability allows the solar panel to deploy and expand.

Shape memory alloys (SMA) are widely used as actuators in special in systems where great displacements are required. Origami structures actuated by SMA have been employed in many works (Peraza-Hernandez *et al*., 2014) and it exhibits promising results. The origami folding operations are usually related to great displacements, what makes the use of SMA as actuators an interesting option. Lee *et al.* (2013) present a robotic wheel actuated by SMA with the ability of changing its radius.

However, the employment of SMA in general systems turns their formulation nonlinear (Paiva and Savi, 2006). Besides, the origami itself has a nonlinear geometry due to the creases. The coupling of the nonlinearities of the structure and of the constitutive model turns the dynamic of origami-SMA systems much intricate. Fonseca *et al*. (2016) present the dynamic analysis of a robotic wheel and rich dynamic responses are noted, including chaos. Another nonlinear analysis is presented by Fang *et al.* (2017), studying the dynamic behavior of Miura-origami structures that have been recently used in metamaterials.

An investigation of the nonlinear dynamics of a self-expandable cylindrical system origami-inspired is presented. This origami structure is first presented by Kuribayashi *et al.* (2006) as a suggestion to a new type of a stent-graft, a tubular medical device used to protect weakened arterial walls in the human body. The origami creases in the cylindrical shaped structure turns it able to fold itself changing its radius, Fig. 1.

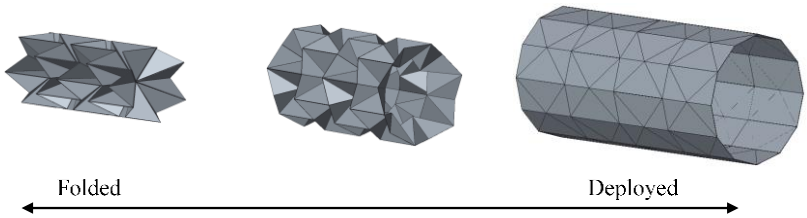

Figure 1. Origami-inspired cylindrical structure deployment (closed on the very left and opened on the very right).

Actuation is provided by torsional shape memory alloy wires placed on the creases and a polynomial constitutive model describe its thermomechanical behavior. A model with two actuators working antagonistically is presented in Rodrigues *et al.* (2017) and this work proposes an actuation with a single actuator presenting Two-Way Shape Memory Effect phenomenon. From the origami geometric relations, a one-degree of freedom system is proposed to represent system dynamics. Numerical simulations considering thermomechanical excitations are carried out showing rich responses.

2. MATHEMATICAL MODELING

The self-folding cylindrical origami studied in this work is constructed by following a folding pattern called waterbomb, which has been applied in many origami-inspired engineering projects (Ma and You, 2014; Hanna *et al.*, 2014). Figure 2 presents a square waterbomb base that is employed repetitively along a paper sheet which extremities are united to mold a cylindrical structure as presented in Fig. 3. Because of the folds, the waterbomb base can go through two stages (Kuribayashi, 2004). In the first stage, every fold line (AC, BC and the symmetric fold lines) is folded whereas in the second stage the fold line BC (and its symmetric fold lines) is not folded and the points A, A_2 and C are co-linear.

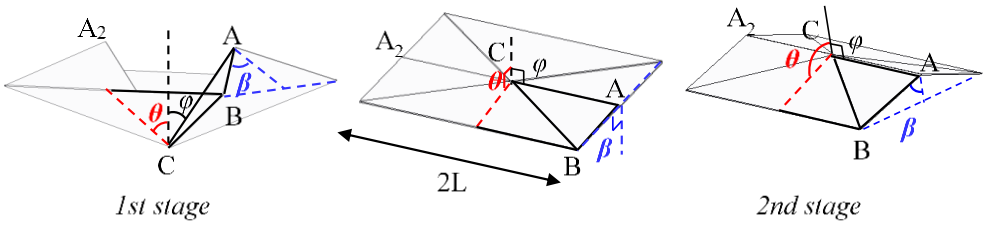

Figure 2. Waterbomb base deployment going through two stages.

Three angles θ, β and φ that characterize the waterbomb base are presented in Fig. 2 and they are geometrically coupled with each other. The angle θ is elected as the angle of deployment and the other angles are so described in function of θ. The first stage is then defined as when $\theta < \pi$ and the second stage as when $\theta \geq \pi/2$. Figure 3 presents the cylindrical structure deployment where the two images on the left represent the structure on the first stage and the image on the very right represents the structure on the second stage.

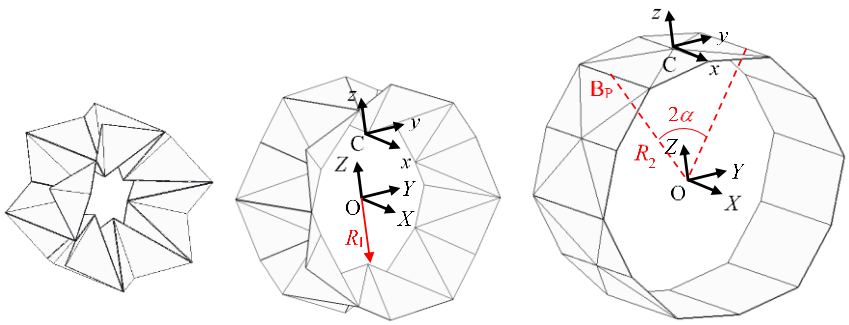

Figure 3. Origami cylindrical structure deployment (1st stage on the left and 2nd stage on the right).

The whole origami is analyzed based on a single squared cell element (waterbomb base). For that, some hypotheses are established: the facets of the elements remain straight, the fold movement occurs only in the creases; and the structure is symmetric then all the elements behave equally and the element itself is symmetric. Thus, one-quarter of the cell element can be taken into account. Under these hypotheses and electing θ as deployment angle, the geometric relations of the angles are described hereafter and they are naturally different in each stage.

On the first stage, let us consider the position of the points A and B on the (x,y,z) system with origin on C (Fig. 2 and Fig. 3): A = (Lsin(φ), 0, Lcos(φ)) and B = (L, Lsin(θ), Lcos(θ)). Because the distance AB = L, it follows that:

$$1 = \sin(\varphi) + \cos(\varphi)\cos(\theta) \tag{1}$$

Solving Eq. (1) for φ, one solution is written below, which describes the evolution of φ in function of θ:

$$\varphi = \operatorname{asin}\left(\frac{1-\cos^2(\theta)}{1+\cos^2(\theta)}\right) \tag{2}$$

By triangle similarity, it is possible to find that the angle β has the same value of the angle θ during the first stage (Kuribayahsi, 2004; Rodrigues *et al.*, 2017).

On the second stage, it is easy to determine the relations between θ and φ and between θ and β by looking the Fig. 2. The angle φ remains constant during this stage and equal to $\pi/2$ and $\beta = \pi - \theta$.

In resume, the geometric relations between the angles are:

$$\beta = \begin{cases} \theta & \text{if } \theta < \pi/2 \\ \pi - \theta & \text{if } \pi/2 \le \theta \end{cases} \tag{3}$$

$$\varphi = \begin{cases} \operatorname{asin}\left(\dfrac{1-\cos^2(\theta)}{1+\cos^2(\theta)}\right) & \text{if } \theta < \pi/2 \\ \pi/2 & \text{if } \pi/2 \le \theta \end{cases} \tag{4}$$

Let O be the central point of the cylindrical structure. An internal radius R_1 is defined as OC and an external radius R_2 is defined as OB_P (Fig. 3). Let n be the number of cells distributed circumferentially. According to the hypotheses, the central angle α is constant and equal to π/n. Thus, Fig. 3 furnishes the following relations:

$$R_1 = \frac{L\sin(\theta)}{\tan(\pi/n)} - L\cos(\theta) \tag{5}$$

$$R_2 = \frac{L\sin(\theta)}{\sin(\pi/n)} \tag{6}$$

The definition of these radii are important to describe the geometric limits of the origami structure. The internal radius cannot be less than zero and, besides that, it cannot be greater than the external radius. It reveals that there is a range for θ where out of it the structure would collapse. Equaling $R_1 = 0$ and $R_1 = R_2$, the limit angles $\theta_{\min}$ and $\theta_{\max}$ are respectively found:

$$\theta_{\min} = \pi/n \tag{7}$$

$$\theta_{\max} = \pi(n+1)/(2n) \tag{8}$$

2.1 Kinematics and Dynamical analysis

On kinematics analyses, rotations of two triangles of one-quarter of the cell are considered: triangle ABC that rotates φ and β and triangle BB_PC that rotates θ (Fig. 4). Let F be the global coordinate frame (X,Y,Z) with origin on O, as in Fig. 3. The coordinate frame P(x,y,z) with origin on C follows the translation on the radial direction of the cell element. Three others coordinates frames with origin on C are defined, each one associate to an angle rotation: Q($x^{(1)}$,$y^{(1)}$,$z^{(1)}$) for

φ, R($x^{(2)}$,$y^{(2)}$,$z^{(2)}$) for β and S($x^{(3)}$,$y^{(3)}$,$z^{(3)}$) for θ (Fig. 4). Transformation matrix can be constructed based on these rotations.

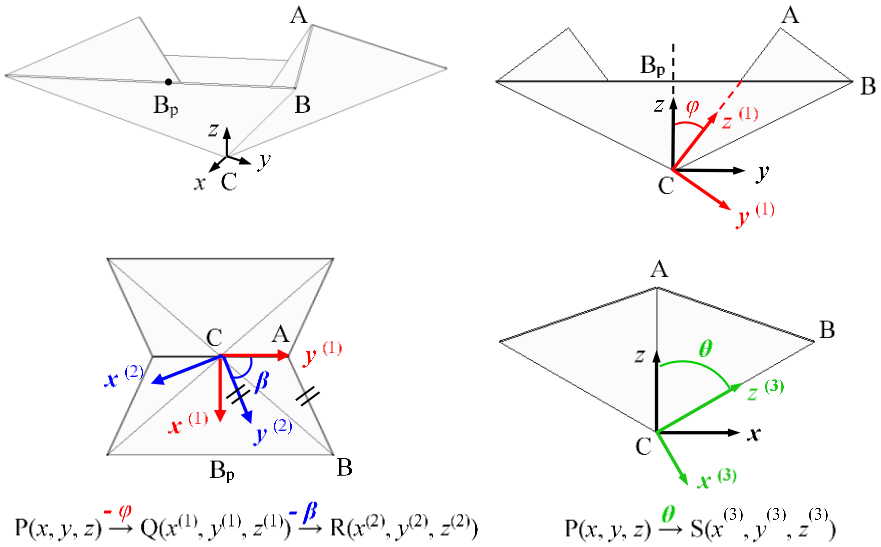

Figure 4. Coordinate frames associate to the rotation angles in the waterbomb base.

Each triangle, ABC and BBPC, presents a rotation inertia as below:

$$ {}^{R}\boldsymbol{I}_{ABC} = m_{ABC}\begin{bmatrix} \frac{4}{3}L^2 & 0 & 0 \\ 0 & \frac{1}{2}L^2 & -\frac{1}{4}L^2 \\ 0 & -\frac{1}{4}L^2 & \frac{1}{6}L^2 \end{bmatrix} \tag{9} $$

$$ {}^{S}\boldsymbol{I}_{BBpC} = m_{BBpC}\begin{bmatrix} \frac{4}{3}L^2 & 0 & 0 \\ 0 & \frac{1}{2}L^2 & -\frac{1}{4}L^2 \\ 0 & -\frac{1}{4}L^2 & \frac{1}{6}L^2 \end{bmatrix} \tag{10} $$

The triangle angular velocities represented in the global coordinate frame are:

$$ {}^{F}\boldsymbol{\omega}_{ABC} = \begin{bmatrix} \dot{\varphi} \\ \sin(\varphi)\dot{\beta} \\ \cos(\varphi)\dot{\beta} \end{bmatrix} \tag{11} $$

$$ {}^{F}\boldsymbol{\omega}_{BBpC} = \begin{bmatrix} 0 \\ \dot{\theta} \\ 0 \end{bmatrix} \tag{12} $$

Besides the rotation inertia, each triangle, ABC and BBPC, has a lumped mass m_1 and m_2 located in their centroid r_1 and r_2, respectively. These concentrated masses are associated to linear velocities given by:

$$ {}^{F}\boldsymbol{v}_1 = \frac{d}{dt}\left[{}^{F}\boldsymbol{T}^{Q}\,{}^{Q}\boldsymbol{T}^{R}\,{}^{R}_{C}\boldsymbol{r}_1 \right] = \begin{bmatrix} \frac{1}{3}L\cos(\beta)\dot{\beta} \\ -\frac{1}{3}L\sin(\beta)\cos(\varphi)\dot{\beta} - \left(\frac{1}{3}L\cos(\beta)\sin(\varphi) - \frac{2}{3}L\cos(\varphi)\right)\dot{\varphi} \\ +\frac{1}{3}L\sin(\beta)\sin(\varphi)\dot{\beta} - \left(\frac{1}{3}L\cos(\beta)\cos(\varphi) + \frac{2}{3}L\sin(\varphi)\right)\dot{\varphi} + \dot{R}_1 \end{bmatrix} \tag{13} $$

$$ {}^{F}\boldsymbol{v}_2 = \frac{d}{dt}\left[{}^{F}\boldsymbol{T}^{S}\,{}^{S}_{C}\boldsymbol{r}_2 \right] = \begin{bmatrix} \frac{2}{3}L\cos(\theta)\dot{\theta} \\ 0 \\ -\frac{2}{3}L\sin(\theta)\dot{\theta} + \dot{R}_1 \end{bmatrix} \tag{14} $$

In order to write an equivalent 1-DOF system to represent the origami dynamics, the kinetic energy is written as follows:

$$ E = \frac{1}{2}m_1\boldsymbol{v}_1\boldsymbol{v}_1 + \frac{1}{2}m_2\boldsymbol{v}_2\boldsymbol{v}_2 + \frac{1}{2}\left(\boldsymbol{\omega}_{ABC}\right)^{T}\boldsymbol{I}_{ABC}\boldsymbol{\omega}_{ABC} + \frac{1}{2}\left(\boldsymbol{\omega}_{BBpC}\right)^{T}\boldsymbol{I}_{BBpC}\boldsymbol{\omega}_{BBpC} \tag{15} $$

The actuation is provided by a torsion SMA wire with length L_S and radius r_S (Koh *et al.*, 2014). It is placed on each side of a cell element on the crease AC (Fig. 5). The constitutive model used to describe the SMA thermomechanical behavior is based on a polynomial model (Falk, 1980) and the torque-displacement relation is Eq. (16). The terms a_1, a_2 and a_3 are material constants, the polar inertia is $J = \pi r_s^4/2$, θ_I is the angle of null tension, T is the temperature and T_M is the temperature below which the martensitic phase is stable (and analogously, T_A is the temperature above which the austenitic phase is stable). An additional constant term σ_P is added from the original polynomial model to contemplate the Two-Way Shape Memory Effect phenomenon.

$$ M_{SMA} = \frac{J}{r_s}\left[a_1\left(T - T_M\right)\left(2\frac{r_s}{L_s}\theta - 2\frac{r_s}{L_s}\theta_I\right) - a_2\left(2\frac{r_s}{L_s}\theta - 2\frac{r_s}{L_s}\theta_I\right)^3 + a_3\left(2\frac{r_s}{L_s}\theta - 2\frac{r_s}{L_s}\theta_I\right)^5 - \sigma_P \right] \tag{16} $$

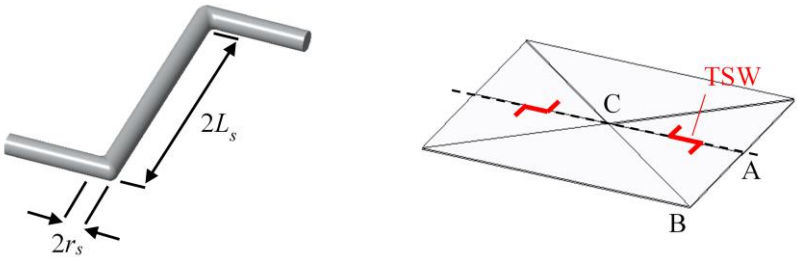

Figure 5. Torsional SMA actuator with two-way shape memory effect placed on the crease AC.

Considering an external force Q_{ext} applied on the point C and in the radial direction and a linear viscous dissipative term ζ, equation of motion is then obtained from Lagrange's equation:

$$ \frac{\partial}{\partial t}\left(\frac{\partial E}{\partial \dot{\theta}}\right) - \left(\frac{\partial E}{\partial \theta}\right) = -\zeta\dot{\theta} - \frac{1}{2}M_{SMA}(\theta) + Q_{ext}\frac{\partial R_1}{\partial \theta} \tag{17} $$

However, the geometric limitations presented previously must be included in the dynamical formulation as well. For that, an extra generalized force is added that limit θ to vary in the range $[\theta_{min}, \theta_{max}]$ and it is expressed as a moment M_{lim} of the form:

$$M_{lim}(\theta)=\begin{cases}k_{lim}(\theta-\theta_{min}) & ,\text{if } \theta<\theta_{min}\\ 0 & ,\text{if } \theta_{min}\le\theta\le\theta_{max}\\ k_{lim}(\theta-\theta_{max}) & ,\text{if } \theta>\theta_{max}\end{cases} \tag{18}$$

Eq. (18) is introduced on the right-hand side in Eq. (17) with the same signal of the torque M_{SMA} of the SMA element. The left-hand side of Eq. (17) can be simplified to $g_1(\theta)\ddot{\theta}+g_2(\theta)\dot{\theta}^2$, where $g_1(\theta)$ and $g_2(\theta)$ are nonlinear functions originated from the derivative of the kinetic energy and represent the nonlinearities of the origami structure. These functions are not explicitly expressed here because of their complexity, but it can be easily found from Eq. (15) and Eq. (17).

Applying these modifications in Eq. (17) and putting it in a dimensionless form (dividing it by $m_1L^2\omega_R{}^2$, being ω_R a reference frequency, $\omega_R=\sqrt{Ja_1T_M/\left(m_1L^2L_S\right)}$ for convenience), the equation of motion Eq. (19) is obtained, where $\tau=\omega t$ is the dimensionless time and $(\ )'=\partial(\ )/\partial\tau$, and therefore $\dot{\theta}=\theta'\omega_R$ and $\ddot{\theta}=\theta''\omega_R{}^2$:

$$\begin{cases}\theta'=v\\ \theta''=-f_1(\theta)v^2-f_2(\theta)\xi v-f_2(\theta)M(\theta)+f_2(\theta)\left(\dfrac{1}{L}\dfrac{\partial R_1}{\partial\theta}\right)F_{ext}\end{cases} \tag{19}$$

where the dimensionless terms are $f_1(\theta)=\dfrac{g_2(\theta)}{g_1(\theta)}$, $f_2(\theta)=\dfrac{m_1L^2}{g_1(\theta)}$, $M(\theta)=\dfrac{M_{SMA}/2+M_{\lim}}{m_1L^2\omega_R{}^2}$, $F_{ext}=\dfrac{Q_{ext}}{m_1L^2\omega_R{}^2}$ and $\xi=\dfrac{\zeta}{m_1L^2\omega_R}$.

The external loads are assumed as harmonic loads in this paper. For such purpose, Eq. (20) describes the dimensionless external force and Eq. (21) describes a thermal oscillation around a temperature T_f:

$$F_{ext}=\mu\sin(\Omega\tau) \tag{20}$$

$$T=T_f+\mu_T\sin(\Omega_T\tau) \tag{21}$$

3. NUMERICAL SIMULATIONS

The dynamic behavior of the cylindrical origami system actuated by torsion SMA wires is analyzed. Numerical simulations are carried out by employing the fourth-order Runge-Kutta method. Table 1 presents the system parameters employed considering a square element and $\xi = 0.3$. With these parameters, the reference frequency is $\omega_R = 62{,}09$ rad/s. The reference temperature $T_0 = 293{,}15$ K is where the system is in equilibrium in a chosen folded configuration of $\theta = \theta_0 = \pi/6$. Aiming a better comprehension, results in the figures are presented in degrees.

Table 1. Parameters of the simulations.

$m_1 = m_{ABC}$ (kg)	$m_2 = m_{BBpC}$ (kg)	r_s (m)	L_s (m)	L (m)	θ_I
5×10^{-5}	$5 \times 0\ 10^{-5}$	$8{,}0 \times 10^{-5}$	$2{,}2 \times 10^{-3}$	$6{,}6 \times 10^{-3}$	$\pi/2$
a_1 (MPa/K)	a_2 (MPa)	a_3 (MPa)	σ_P	T_M	T_A
$1{,}0 \times 10^{6}$	$1{,}4 \times 10^{10}$	$2{,}26 \times 10^{12}$	0,06	287,15	308,9

Because it is trained to present a two-way shape memory effect, the SMA actuator is responsible for both opening and closing processes of the structure. These processes must occur only with the temperature changes. A thermal load is applied to the structure at the reference configuration and the changes occurred are analyzed for origamis with different number n of elements in Fig. 6.

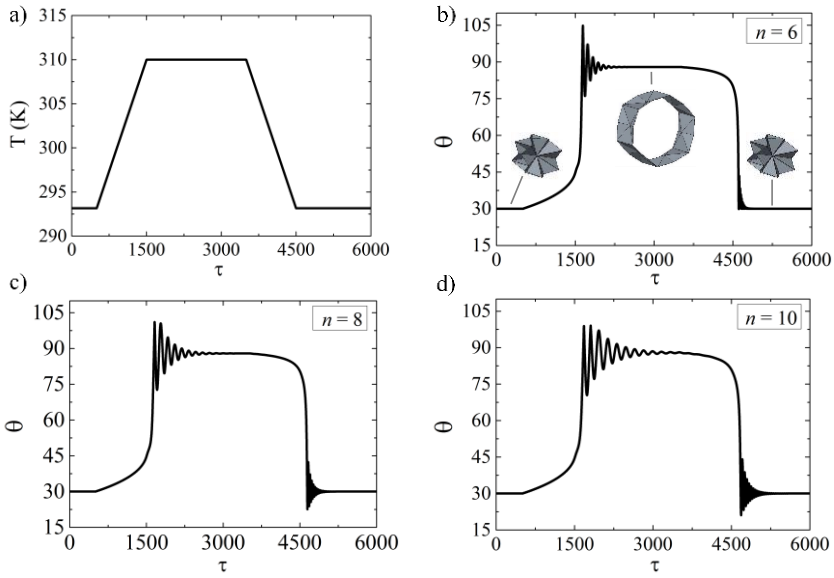

Figure 6. Opening and closing processes due to a thermal load.

A thermal load is presented in Fig. 6a. The temperature is initially at the reference temperature T_0 and it increases until T = 310 K, a temperature above T_A, and then it decreases until T_0 again. The deployment angle θ in function of the time τ during this thermal load is presented in Fig. 6b – Fig. 6d. As the temperature increases, the angle also increases which means that the structure opens; and as the temperature decreases, the angle also decreases and then the structure closes. After opening or closing, a vibration is noted. This vibration takes more time to attenuate if the number of elements is higher. Besides, a change in the number of elements modifies the natural frequency of these vibrations, being lower to greater values of n.

The results in Fig. 6 validates the two-way shape memory effect in the origami system, then it is possible to activate the structure to reach a opened configuration only by changing its temperature. One can assumes the opened configuration as the configuration of operation where the structure could be subjected to different loads.

Figure 7 presents a thermal oscillation after heating the structure to the opened configuration, that is, in the operational configuration. This oscillation of 2 K of amplitude influences the dynamical response with an oscillatory response. However, this influence is small and it is smaller for greater number of elements.

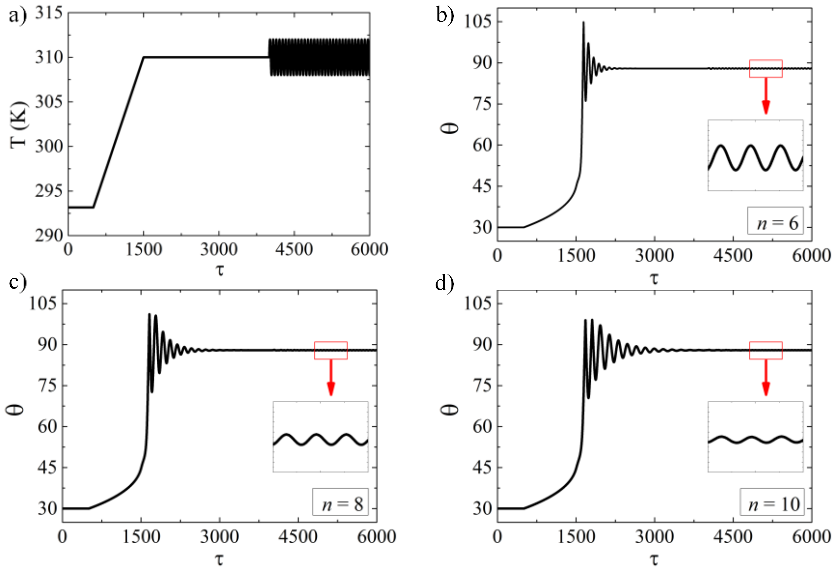

Figure 7. Influence of a thermal oscillation in the operational configuration (opened configuration).

Considering again the opened configuration (high temperature, T = 310 K) as a configuration of operation, let us assume a mechanical load, Eq. (20). A global analysis is performed presenting bifurcation diagrams that represent a stroboscopic view of system dynamics under the slow variation of a parameter. The amplitude μ of the harmonic force is analyzed under the frequency of Ω = 0,30. The dimensionless coefficient μ is varied to 0,01 until 0,8, which corresponds to a force in the order of magnitude of 10^{-4} N by assuming the values of Table 1.

Figure 8 presents bifurcation diagrams for n = 6, n = 8 and n = 10. Some similarities can be noted in the bifurcation diagrams: for small force amplitudes, the system presents in general a periodic-1 response; after that, a cloud of points suggest a quasi-periodic or chaotic response; then, bifurcations start from chaotic-like response to period-1 response; a period-1 response is predominant until the force amplitude is high enough and the system response becomes chaotic.

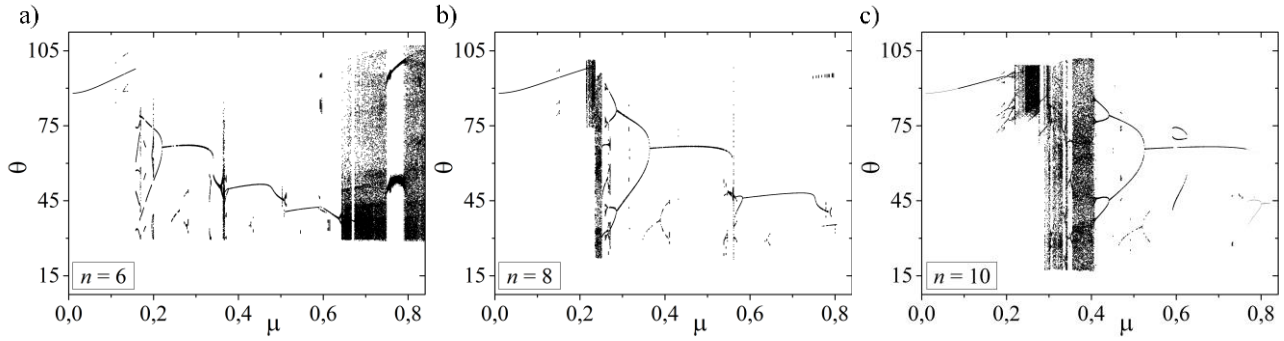

Figure 8. Bifurcation diagrams for Ω = 0,3 and varying μ: a) n = 6; b) n = 8; c) n = 10.

Table 2 gives the range of μ for each general system behavior. The same characteristics are found for greater values of μ if the number n of elements increases. Table 2 is conditioned to the range of the bifurcation diagrams, i.e., from 0,01 to 0,8. For n = 6, a predominantly chaotic response is obtained for μ > 0,643, but for n = 8 and n = 10 it may occurs for μ > 0,8.

Table 2. Range of values of μ for each general behavior found in the bifurcation diagrams.

	n = 6	n = 8	n = 10
mostly periodic-1	0,01 to 0,157	0,01 to 0,214	0,01 to 0,219
cloud of points	0,157 to 0,170	0,214 to 0,259	0,219 to 0,401
bifurcation from chaos	0,170 to 0,221	0,259 to 0,364	0,401 to 0,526
mostly periodic-1	0,221 to 0,643	0,364 to 0,8	0,526 to 0,8

Figure 9 presents the phase-space (black lines) and the Poincaré section (red points) for four values of μ considering n = 10 to exemplify the behaviors found on the diagram bifurcation. For μ = 0,145, the response is periodic-1 and it oscillates around π/2, the opened configuration. A periodic-3 response is found for μ = 0,200 and it is important to note the straight line on the right side of Fig. 6b, which indicates the limit angle θ_{max} is reached. A chaotic motion is obtained for μ = 0,360 and a periodic-1 motion is obtained for μ = 0,700. In both last cases, the limit angles are reached.

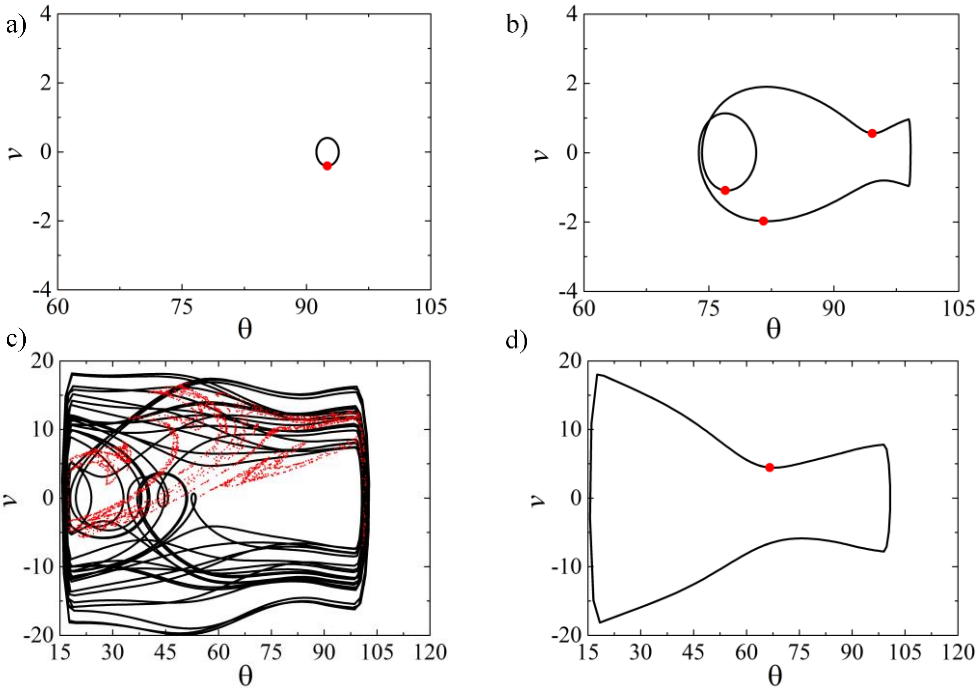

Figure 9. Structure response under a mechanical load of Ω = 0,3 considering n = 10: a) μ = 0,145; b) μ = 0,200; c) μ = 0,360; d) μ = 0,700.

In operational conditions, a thermal oscillation can occur together with the mechanical load. Figure 10 presents the influence of a thermal oscillation in the dynamical response. The responses due to a mechanical load of μ = 0,145 are presented Fig. 7a, Fig. 7b and Fig. 7c for n = 6, n = 8 and n = 10, respectively. If a thermal oscillation of 2 K is applied in each case, the responses are presented in Fig. 7d, Fig. 7e and Fig. 7f, respectively. For n = 6, a change in the periodicity is noted. The amplitude response increases for n = 8 and the limit angle is reached. For n = 10, no considerable changes are noticed.

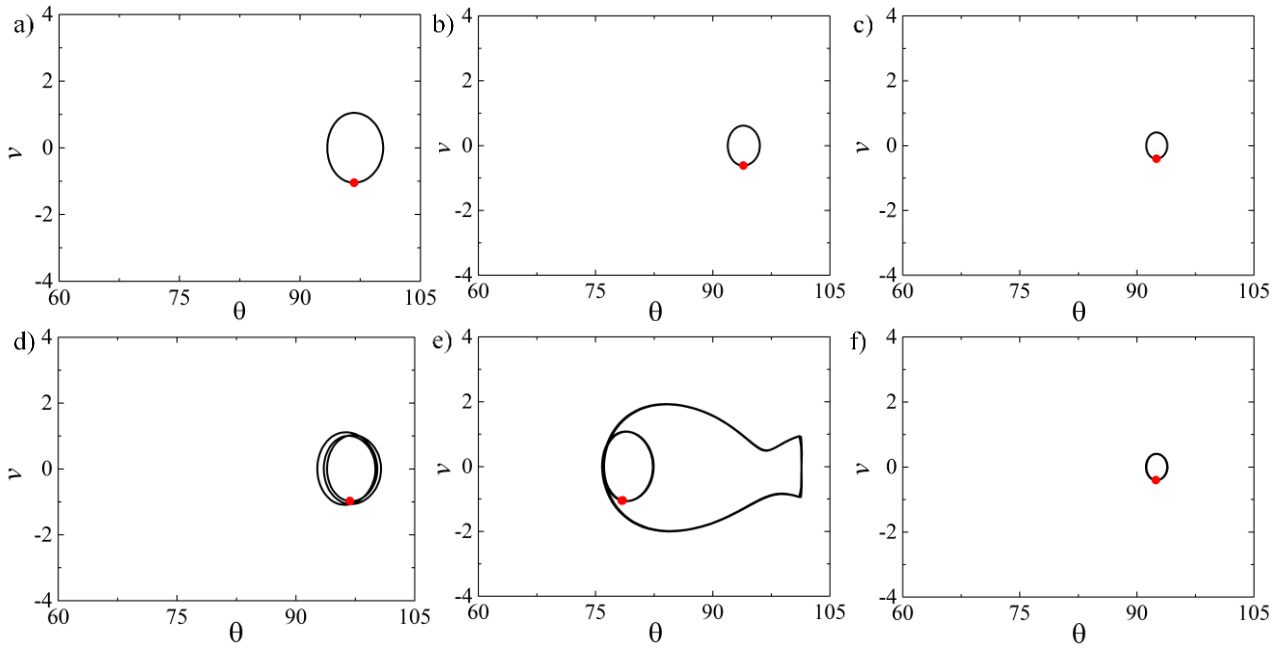

Figure 10. Structure response under a mechanical load of μ = 0,145 and Ω = 0,3. Images a) to c) do not consider a thermal oscillation while images d) to f) consider a thermal oscillation of μ_T = 2 and Ω_T = 0,1: n = 6 to images a) and d); n = 8 to images b) and e); and n = 10 to images c) and f).

4. FINAL REMARKS

This paper presents a nonlinear dynamical analysis of an origami-inspired self-folding cylindrical structure actuated by SMA. A polynomial constitutive model is employed to describe the thermomechanical behavior of the actuator and from the geometrical relations a 1-DOF non-smooth system is built. Results presented show the constitutive model employed allows the structure to change its radius in an opening or closing process only by changing its temperature. Numerical simulations are also carried out showing thermomechanical loads representing operational conditions. The constitutive and geometrical nonlinearities are responsible for rich dynamics, including chaos. From the bifurcation diagrams, these situations of complexness are obtained for greater force amplitudes if the number of cell elements is higher. Thermal oscillations produce a small variation in free vibration. However, together with a mechanical load, these thermal oscillations can change the periodicity of the system or even amplify the dynamical response to a critical situation.

5. ACKNOWLEDGEMENTS

The authors would like to acknowledge the support of the Brazilian Research Agencies CNPq, CAPES and FAPERJ. The Air Force Office of Scientific Research (AFOSR) is also acknowledged.

6. REFERENCES

Falk, F., 1980. “Model free energy, mechanics, and thermodynamics of shape memory alloys”. *Acta Metallurgica*, Vol. 28(12), p. 1773-1780.

Fang, H., Li, S., Ji, H. and Wang, K.W., 2017. “Dynamics of a bistable Miura-origami strucutre”. *Physical Review E*, Vol. 95, p. 052211.

Fonseca, L.M., Rodrigues, G.V., Savi, M.A. and Paiva, A., 2016. “Nonlinear Dynamics of an Origami Strucutre Coupled to Smart Materials”. In *6th International Conference on Nonlinear Science and Complexity – NSC 2016*. São Paulo, Brazil.

Hanna, B.H., Lund, J.M., Lang, R.J., Magleby, S.P. and Howell, L.L., 2014. “Waterbomb base: a symmetric single-vertex bistable origami mechanism”. *Smart Materials and Strucutres*, Vol. 23(9), p. 094009.

Koh, J.S., Kim, S.R. and Cho, K.J., 2014. “Self-folding origami using torsion shape memory alloy wire actuators”. In *International Design Engineering Technical Conferences and Computers and Information in Engineering Conference – IDETC/CIE 2014*. New York, USA.

Kuribayashi, K., 2014. *A novel foldable stent graft*. Ph.D. thesis, University of Oxford, Oxford.

Kuribayashi, K., Tsuchiya, K., You, Z., Tomus, D., Umemoto, M., Ito, T. and Sasaki, M., 2006. “Self-deployable origami stent grafts as a biomedical application of Ni-rich TiNi shape memory alloy foil”. *Materials Science and Engeinnering: A*, Vol. 419(1), p. 131-137.

Lee, D., Kim, J., Kim, S.R., Koh, J.S. and Cho, K.J., 2013. “The deformable wheel robot using magic-ball origami strucuture”. In *International Design Engineering Technical Conferences and Computers and Information in Engineering Conference – IDETC/CIE 2013*. Oregon, USA.

Ma, J. and You, Z., 2014. “Modeling of the waterbomb origami pattern and its applications”. In *International Design and Engineering Technical Conferences and Computers and Information in Engineering Conference – IDETC/CIE 2014*. New York, SUA.

Miura, K., 1994. “Map fold a la miura style, its physical characteristics and application to the space science”. In *Research of Pattern Formation*. Tokyo, Japan.

Paiva, A. and Savi, M.A., 2006. “An overview of constitutive models for shape memory alloys”. *Mathematical Problems in Engineering*, Vol. 2006, p. e56876.

Peraza-Hernandez, E.A., Hartl, D.J., Malak, R.J. and Lagoudas, D.C. “Origami inspired active structures: a synteshis and review”. *Smart Materials and Structures*, Vol. 23, p. 094001.

Rodrigues, G.V., Fonseca, L.M., Savi, M.A. and Paiva, A., 2017. “Nonlinear dynamics of an adaptive origami-stent system”. *International Journal of Mechanical Sciences*, Vol. 133C, p. 303-318.

7. RESPONSIBILITY NOTICE

The authors are the only responsible for the printed material included in this paper.